

Superfluid Weight, Free Carrier Density, and Specific Heat of the $d = 3$ tJ Model at Finite Temperatures

Michael Hinczewski and A. Nihat Berker

*Department of Physics, Istanbul Technical University, Maslak 34469, Istanbul, Turkey,
Department of Physics, Massachusetts Institute of Technology, Cambridge, Massachusetts 02139, U.S.A., and
Feza Gürsey Research Institute, TÜBİTAK - Bosphorus University, Çengelköy 81220, Istanbul, Turkey*

The superfluid weight, free carrier density, and specific heat of the three-dimensional tJ model are calculated by renormalization-group theory. We find that optimal hole doping for superfluidity occurs in the electron density range of $\langle n_i \rangle \approx 0.63$ – 0.68 , where the superfluid weight n_s/m^* reaches a local maximum. This density range is within the novel τ phase, where the electron hopping strength renormalizes to infinity, the system remains partially filled at all length scales, and the electron-hopping expectation value remains distinctively non-zero at all length scales. The calculated superfluid weight drops off sharply in the overdoped region. Under hole doping, the calculated density of free carriers increases until optimal doping and remains approximately constant in the overdoped region, as seen experimentally in high- T_c materials. Furthermore, from calculation of the specific heat coefficient γ , we see clear evidence of a gap in the excitation spectrum for the τ phase.

PACS numbers: 74.72.-h, 71.10.Fd, 05.30.Fk, 74.25.Dw

I. INTRODUCTION

The variation of the superfluid number density n_s with temperature and carrier doping is of fundamental importance in describing the unique properties of the superconducting state in high- T_c cuprates. Experimentally, muon-spin-rotation techniques are used to determine the closely related quantity n_s/m^* (also known as the superfluid weight), where m^* is the effective mass of the carriers in the superfluid. In the underdoped region of high- T_c materials, n_s/m^* increases with doping, and the low-temperature superfluid weight is correlated with T_c . [1, 2] As the materials are doped past the optimal value (where T_c is the highest), n_s/m^* peaks and rapidly decreases. [3, 4, 5] The decrease in n_s/m^* is surprising since the total density of free carriers saturates at optimal doping and remains almost constant in the overdoped region. [6] By contrast, in a conventional superconductor, described by BCS theory, these two quantities have the same doping dependence.

The tJ model is a promising starting point in understanding these properties of cuprate superconductors. Mean-field $U(1)$ and $SU(2)$ slave-boson theories of the tJ Hamiltonian have reproduced some aspects of the doping and temperature dependences of n_s/m^* . [7, 8] More direct, unbiased numerical techniques applied to a 4×4 tJ cluster have observed a large peak in n_s/m^* in the same region where pairing correlations indicate a superconducting ground state. [9] A general limitation of these types of studies is that no finite-cluster approach can unambiguously identify phase transitions in the system, or exhibit the non-analytic behavior of thermodynamic quantities at these transitions.

Alternatively, the physics of the bulk model can be studied through the position-space renormalization-group method, which has been used to determine the phase structure and thermodynamic properties of the tJ and Hubbard models at finite temperatures. [10, 11,

12, 13] In particular, Falicov and Berker's calculation for the tJ model in $d = 3$ with the realistic coupling $J/t = 0.444$ produced a rich, multicritical phase diagram [10, 11], with a novel low-temperature phase (called " τ ") for 30 – 40% hole doping where the electron hopping strength in the Hamiltonian renormalizes to infinity under repeated scale changes, while the system remains partially filled. This is the possible signature of a superconducting phase, and it is notable that a similar phase was also observed in the $d = 3$ Hubbard model. [12, 13]

Our present study further develops this renormalization-group method, to yield the superfluid weight of the tJ model as a function of temperature and hole doping. Our approach reproduces phenomenological features of high- T_c materials. In particular we find that optimal doping is located in the vicinity of the τ phase, where n_s/m^* peaks and then is sharply reduced with overdoping. Moreover, we also find that the density of free carriers increases until optimal doping, and saturates in overdoped region. These results suggest that the τ phase might indeed correspond to the superconducting phase in cuprates. Further supporting this idea, we present specific heat calculations that show clear evidence of a gap in the quasiparticle spectrum for the τ phase.

II. THE tJ HAMILTONIAN

We consider a d -dimensional hypercubic lattice where the tJ model for electron conduction is defined by the

Hamiltonian

$$H = P \left[\tilde{t} \sum_{\langle ij \rangle, \sigma} \left(c_{i\sigma}^\dagger c_{j\sigma} + c_{j\sigma}^\dagger c_{i\sigma} \right) + \tilde{J} \sum_{\langle ij \rangle} \mathbf{S}_i \cdot \mathbf{S}_j - \tilde{V} \sum_{\langle ij \rangle} n_i n_j - \tilde{\mu} \sum_i n_i \right] P, \quad (1)$$

where $c_{i\sigma}^\dagger$ and $c_{i\sigma}$ are creation and annihilation operators, obeying anticommutation rules, for an electron with spin $\sigma = \uparrow$ or \downarrow at lattice site i , $n_{i\sigma} = c_{i\sigma}^\dagger c_{i\sigma}$, $n_i = n_{i\uparrow} + n_{i\downarrow}$ are the number operators, and $\mathbf{S}_i = \sum_{\sigma\sigma'} c_{i\sigma}^\dagger \mathbf{s}_{\sigma\sigma'} c_{i\sigma'}$ is the single-site spin operator, with \mathbf{s} the vector of Pauli spin matrices. The entire Hamiltonian is sandwiched between projection operators $P = \prod_i (1 - n_{i\downarrow} n_{i\uparrow})$, which project out states with doubly-occupied sites. The interaction constants \tilde{t} , \tilde{J} , \tilde{V} describe the following physical features: electron hopping (\tilde{t}), a nearest-neighbor anti-ferromagnetic coupling ($\tilde{J} > 0$), and a nearest-neighbor interaction (\tilde{V}). The standard tJ Hamiltonian is a special case of Eq. (1) with $\tilde{V}/\tilde{J} = 1/4$. For convenience, we introduce dimensionless interaction constants t, J, V, μ , and rearrange the $\tilde{\mu}$ chemical potential term to group the Hamiltonian into a single lattice summation:

$$\begin{aligned} -\beta H &= \sum_{\langle ij \rangle} P \left[-t \sum_{\sigma} \left(c_{i\sigma}^\dagger c_{j\sigma} + c_{j\sigma}^\dagger c_{i\sigma} \right) - JS_i \cdot S_j + V n_i n_j + \mu(n_i + n_j) \right] P \\ &\equiv \sum_{\langle ij \rangle} \{-\beta H(i, j)\}. \end{aligned} \quad (2)$$

Here $\beta = 1/k_B T$, so that the interaction constants are related by $t = \beta \tilde{t}$, $J = \beta \tilde{J}$, $V = \beta \tilde{V}$, $\mu = \beta \tilde{\mu}/2d$. The total Hamiltonian is now written as a sum of pair Hamiltonians $-\beta H(i, j)$. The sum over nearest-neighbor sites (i, j) is taken so that the position of site j is $\mathbf{r}_j = \mathbf{r}_i + \mathbf{a}_k$, where \mathbf{a}_k is one of the d lattice vectors. Since changing the sign of t is equivalent to redefining the phase at every other site in the system, we shall choose $t > 0$ with no loss of generality. The effective temperature variable will be $1/t = k_B T$, where we have taken $\tilde{t} = 1$ as the unit of energy.

In order to study the superfluid weight, we introduce periodic boundary conditions, by considering the system as a ring in each axis direction threaded by a magnetic flux. We choose the vector potential \mathbf{A} associated with the flux to have components A/\sqrt{d} along each axis, so that the pair Hamiltonian becomes

$$\begin{aligned} -\beta H(i, j) &= P \left[-t \sum_{\sigma} \left(e^{i\phi} c_{i\sigma}^\dagger c_{j\sigma} + e^{-i\phi} c_{j\sigma}^\dagger c_{i\sigma} \right) - JS_i \cdot S_j + V n_i n_j + \mu(n_i + n_j) \right] P, \quad (3) \end{aligned}$$

where $\phi = aA/\sqrt{d}$ and a is the lattice spacing. For simplicity, we have adopted units so that $\hbar = c = e = 1$. In the presence of the applied phase twist ϕ , the superfluid weight n_s/m^* is related to the curvature of the total free energy F near $\phi = 0$, [14, 15]

$$\frac{n_s}{m^*} = \frac{1}{Na^2} \lim_{A \rightarrow 0} \frac{\partial^2 F}{\partial A^2} = \frac{1}{Nd} \lim_{\phi \rightarrow 0} \frac{\partial^2 F}{\partial \phi^2}, \quad (4)$$

where $N \rightarrow \infty$ is the total number of lattice sites. In Sec.III E we shall show how this quantity can be calculated from the renormalization-group transformation developed below.

III. RENORMALIZATION-GROUP TRANSFORMATION

A. Recursion Relations

The position-space renormalization-group method used here starts with an approximate decimation in $d = 1$, which is then generalized to higher dimensions by the Migdal-Kadanoff procedure [10, 11]. In $d = 1$, the Hamiltonian of Eq. (2) takes the form:

$$-\beta H = \sum_i \{-\beta H(i, i+1)\}, \quad (5)$$

where $i = 1, 2, 3, \dots$. The decimation consists of finding a thermodynamically equivalent system, described by the Hamiltonian $-\beta' H'$, which depends only on the states of the odd-numbered sites. Since the quantum operators in the Hamiltonian do not commute, an exact decimation even in one dimension is not possible. We can carry out an approximate decimation as follows [16, 17]:

$$\begin{aligned} \text{Tr}_{\text{even}} e^{-\beta H} &= \text{Tr}_{\text{even}} e^{\sum_i \{-\beta H(i, i+1)\}} \\ &= \text{Tr}_{\text{even}} e^{\sum_i^{\text{even}} \{-\beta H(i-1, i) - \beta H(i, i+1)\}} \\ &\simeq \prod_i^{\text{even}} \text{Tr}_i e^{\{-\beta H(i-1, i) - \beta H(i, i+1)\}} \\ &= \prod_i^{\text{even}} e^{-\beta' H'(i-1, i+1)} \\ &\simeq e^{\sum_i^{\text{even}} \{-\beta' H'(i-1, i+1)\}} = e^{-\beta' H'}. \end{aligned} \quad (6)$$

Here $-\beta' H'$ is the Hamiltonian for the renormalized system, and Tr_{even} is a trace over the degrees of freedom at all even-numbered sites. In the two approximate steps, marked by \simeq in Eq. (6), we ignore the non-commutation of operators separated beyond three consecutive sites of the unrenormalized system (conversely, this means that anticommutation rules are taken into account within three consecutive sites at all successive length scales, as the renormalization-group procedure is repeated). These two steps involve the same approximation but in opposite directions, which gives some mutual

compensation. Earlier studies of quantum spin systems have shown the success of this approximation at predicting finite-temperature behavior.[16, 17]

The renormalization-group mapping can be extracted from the third and fourth lines of Eq.(6):

$$e^{-\beta' H'(i,k)} = \text{Tr}_j e^{-\beta H(i,j) - \beta H(j,k)}, \quad (7)$$

where i, j, k are three consecutive sites of the unrenormalized system. The operators $-\beta' H'(i, k)$ and $-\beta H(i, j) - \beta H(j, k)$ act on the space of two-site and three-site states respectively, so that, in terms of matrix elements,

$$\langle u_i v_k | e^{-\beta' H'(i,k)} | \bar{u}_i \bar{v}_k \rangle = \sum_{w_j} \langle u_i w_j v_k | e^{-\beta H(i,j) - \beta H(j,k)} | \bar{u}_i w_j \bar{v}_k \rangle, \quad (8)$$

where $u_i, w_j, v_k, \bar{u}_i, \bar{v}_k$ are single-site state variables. Eq.(8) is the contraction of a 27×27 matrix on the right into a 9×9 matrix on the left. We block-diagonalize the left and right sides of Eq.(8) by choosing basis states which are the eigenstates of total particle number, total spin magnitude, total spin z -component, and parity. We denote the set of 9 two-site eigenstates by $\{|\phi_p\rangle\}$ and the set of 27 three-site eigenstates by $\{|\psi_q\rangle\}$, and list them in Tables I and II. Eq.(8) is rewritten as

$$\langle \phi_p | e^{-\beta' H'(i,k)} | \phi_{\bar{p}} \rangle = \sum_{\substack{u,v,\bar{u}, \\ \bar{v},w}} \sum_{q,\bar{q}} \langle \phi_p | u_i v_k \rangle \langle u_i w_j v_k | \psi_q \rangle \langle \psi_q | e^{-\beta H(i,j) - \beta H(j,k)} | \psi_{\bar{q}} \rangle \langle \psi_{\bar{q}} | \bar{u}_i \bar{w}_j \bar{v}_k \rangle \langle \bar{u}_i \bar{v}_k | \phi_{\bar{p}} \rangle. \quad (9)$$

Eq. (9) yields six independent elements for the matrix $\langle \phi_p | e^{-\beta' H'(i,k)} | \phi_{\bar{p}} \rangle$, which we label γ_p as follows:

$$\begin{aligned} \gamma_p &\equiv \langle \phi_p | e^{-\beta' H'(i,k)} | \phi_p \rangle \quad \text{for } p = 1, 2, 4, 6, 7, \\ \gamma_0 &\equiv \langle \phi_2 | e^{-\beta' H'(i,k)} | \phi_4 \rangle. \end{aligned} \quad (10)$$

To calculate the γ_p , we determine the matrix elements of $-\beta H(i, j) - \beta H(j, k)$ in the three-site basis $\{|\psi_q\rangle\}$, as listed in Table III, and exponentiate the matrix blocks to find the elements $\langle \psi_q | e^{-\beta H(i,j) - \beta H(j,k)} | \psi_{\bar{q}} \rangle$ which enter on the right-hand side of Eq. (9). In this way the γ_p are functions of the interaction constants in the unrenormalized Hamiltonian, $\gamma_p = \gamma_p(t, \phi, J, V, \mu)$.

Since the matrix $\langle \phi_p | e^{-\beta' H'(i,k)} | \phi_{\bar{p}} \rangle$ is determined by six independent elements γ_p , the renormalized pair Hamiltonian $-\beta' H'(i, k)$ involves six interaction constants, namely those of the original types of interactions and an additive constant:

$$\begin{aligned} -\beta' H'(i, k) &= P \left[-t' \sum_{\sigma} \left(e^{i\phi'} c_{i\sigma}^{\dagger} c_{j\sigma} + e^{-i\phi'} c_{j\sigma}^{\dagger} c_{i\sigma} \right) \right. \\ &\quad \left. - J' \mathbf{S}_i \cdot \mathbf{S}_j + V' n_i n_j + \mu' (n_i + n_j) + G' \right] P, \quad (11) \end{aligned}$$

n	p	s	m_s	Two-site basis states
0	+	0	0	$ \phi_1\rangle = \circ\circ\rangle$
1	+	1/2	1/2	$ \phi_2\rangle = \frac{1}{\sqrt{2}}\{ \uparrow\circ\rangle + \circ\uparrow\rangle\}$
1	-	1/2	1/2	$ \phi_4\rangle = \frac{1}{\sqrt{2}}\{ \uparrow\circ\rangle - \circ\uparrow\rangle\}$
2	-	0	0	$ \phi_6\rangle = \frac{1}{\sqrt{2}}\{ \uparrow\downarrow\rangle - \downarrow\uparrow\rangle\}$
2	+	1	1	$ \phi_7\rangle = \uparrow\uparrow\rangle$
2	+	1	0	$ \phi_9\rangle = \frac{1}{\sqrt{2}}\{ \uparrow\downarrow\rangle + \downarrow\uparrow\rangle\}$

TABLE I: The two-site basis states, with the corresponding particle number (n), parity (p), total spin (s), and total spin z -component (m_s) quantum numbers. The states $|\phi_3\rangle$, $|\phi_5\rangle$, and $|\phi_8\rangle$, are obtained by spin reversal from $|\phi_2\rangle$, $|\phi_4\rangle$, and $|\phi_7\rangle$, respectively.

n	p	s	m_s	Three-site basis states
0	+	0	0	$ \psi_1\rangle = \circ\circ\circ\rangle$
1	+	1/2	1/2	$ \psi_2\rangle = \circ\uparrow\circ\rangle, \psi_3\rangle = \frac{1}{\sqrt{2}}\{ \uparrow\circ\circ\rangle + \circ\circ\uparrow\rangle\}$
1	-	1/2	1/2	$ \psi_6\rangle = \frac{1}{\sqrt{2}}\{ \uparrow\circ\circ\rangle - \circ\circ\uparrow\rangle\}$
2	+	0	0	$ \psi_8\rangle = \frac{1}{2}\{ \uparrow\downarrow\circ\rangle - \downarrow\uparrow\circ\rangle - \circ\uparrow\downarrow\rangle + \circ\downarrow\uparrow\rangle\}$
2	-	0	0	$ \psi_9\rangle = \frac{1}{2}\{ \uparrow\downarrow\circ\rangle - \downarrow\uparrow\circ\rangle + \circ\uparrow\downarrow\rangle - \circ\downarrow\uparrow\rangle\},$ $ \psi_{10}\rangle = \frac{1}{\sqrt{2}}\{ \uparrow\circ\downarrow\rangle - \downarrow\circ\uparrow\rangle\}$
2	+	1	1	$ \psi_{11}\rangle = \uparrow\circ\uparrow\rangle, \psi_{12}\rangle = \frac{1}{\sqrt{2}}\{ \uparrow\uparrow\circ\rangle + \circ\uparrow\uparrow\rangle\}$
2	+	1	0	$ \psi_{13}\rangle = \frac{1}{2}\{ \uparrow\downarrow\circ\rangle + \downarrow\uparrow\circ\rangle + \circ\uparrow\downarrow\rangle + \circ\downarrow\uparrow\rangle\},$ $ \psi_{14}\rangle = \frac{1}{\sqrt{2}}\{ \uparrow\circ\downarrow\rangle + \downarrow\circ\uparrow\rangle\}$
2	-	1	1	$ \psi_{17}\rangle = \frac{1}{\sqrt{2}}\{ \uparrow\uparrow\circ\rangle - \circ\uparrow\uparrow\rangle\}$
2	-	1	0	$ \psi_{18}\rangle = \frac{1}{2}\{ \uparrow\downarrow\circ\rangle + \downarrow\uparrow\circ\rangle - \circ\uparrow\downarrow\rangle - \circ\downarrow\uparrow\rangle\}$
3	+	1/2	1/2	$ \psi_{20}\rangle = \frac{1}{\sqrt{6}}\{2 \uparrow\uparrow\uparrow\rangle - \uparrow\uparrow\downarrow\rangle - \uparrow\downarrow\uparrow\rangle\}$
3	-	1/2	1/2	$ \psi_{22}\rangle = \frac{1}{\sqrt{2}}\{ \uparrow\uparrow\downarrow\rangle - \downarrow\uparrow\uparrow\rangle\}$
3	+	3/2	3/2	$ \psi_{24}\rangle = \uparrow\uparrow\uparrow\rangle$
3	+	3/2	1/2	$ \psi_{25}\rangle = \frac{1}{\sqrt{3}}\{ \uparrow\uparrow\downarrow\rangle + \uparrow\downarrow\uparrow\rangle + \downarrow\uparrow\uparrow\rangle\}$

TABLE II: The three-site basis states, with the corresponding particle number (n), parity (p), total spin (s), and total spin z -component (m_s) quantum numbers. The states $|\phi_{4-5}\rangle$, $|\phi_7\rangle$, $|\phi_{15-16}\rangle$, $|\phi_{19}\rangle$, $|\phi_{21}\rangle$, $|\phi_{23}\rangle$, $|\phi_{26-27}\rangle$, are obtained by spin reversal from $|\phi_{2-3}\rangle$, $|\phi_6\rangle$, $|\phi_{11-12}\rangle$, $|\phi_{17}\rangle$, $|\phi_{20}\rangle$, $|\phi_{22}\rangle$, $|\phi_{24-25}\rangle$, respectively.

The matrix elements of $-\beta' H'(i, k)$ in the $\{\phi_p\}$ basis are shown in Table IV. Exponentiating this matrix, we can solve for the renormalized interaction constants ($t', \phi', J', V', \mu', G'$) in terms of the γ_p :

$$\begin{aligned} t' &= \text{sign}(\gamma_4 - \gamma_2) \cosh^{-1} \left(\frac{\gamma_2 + \gamma_4}{2e^v} \right), \\ \phi' &= \tan^{-1} \left(\frac{2 \text{Im} \gamma_0}{\gamma_4 - \gamma_2} \right), \quad J' = \ln \frac{\gamma_7}{\gamma_6}, \\ V' &= \frac{1}{4} \{ \ln(\gamma_1^4 \gamma_6 \gamma_7^3) - 8v \}, \quad \mu' = v - \ln \gamma_1, \\ G' &= \ln \gamma_1, \end{aligned} \quad (12)$$

where

$$v = \frac{1}{2} \ln(\gamma_2 \gamma_4 - \gamma_0^* \gamma_0).$$

The approximate $d = 1$ decimation contained in Eqs. (9)-(12) can be expressed as a mapping of a Hamil-

	ψ_1
ψ_1	0

	ψ_2	ψ_3	ψ_6
ψ_2	2μ	$-\sqrt{2}t \cos \phi$	$i\sqrt{2}t \sin \phi$
ψ_3	$-\sqrt{2}t \cos \phi$	μ	$i\Delta_1$
ψ_6	$-i\sqrt{2}t \sin \phi$	$-i\Delta_1$	μ

	ψ_8	ψ_9	ψ_{10}
ψ_8	$-\frac{3}{4}J + V + 3\mu$	$-i\Delta_3$	$-i\sqrt{2}t \sin \phi$
ψ_9	$i\Delta_3$	$-\frac{3}{4}J + V + 3\mu$	$-\sqrt{2}t \cos \phi$
ψ_{10}	$i\sqrt{2}t \sin \phi$	$-\sqrt{2}t \cos \phi$	2μ

	ψ_{11}	ψ_{12}	ψ_{17}
ψ_{11}	2μ	$-\sqrt{2}t \cos \phi$	$i\sqrt{2}t \sin \phi$
ψ_{12}	$-\sqrt{2}t \cos \phi$	$\frac{1}{4}J + V + 3\mu$	$i\Delta_2$
ψ_{17}	$-i\sqrt{2}t \sin \phi$	$-i\Delta_2$	$\frac{1}{4}J + V + 3\mu$

	ψ_{13}	ψ_{14}	ψ_{18}
ψ_{13}	$\frac{1}{4}J + V + 3\mu$	$-\sqrt{2}t \cos \phi$	$i\Delta_4$
ψ_{14}	$-\sqrt{2}t \cos \phi$	2μ	$i\sqrt{2}t \sin \phi$
ψ_{18}	$-i\Delta_4$	$-i\sqrt{2}t \sin \phi$	$\frac{1}{4}J + V + 3\mu$

	ψ_{20}	ψ_{22}
ψ_{20}	$-J + 2V + 4\mu$	$2V + 4\mu$

	ψ_{24}	ψ_{25}
ψ_{24}	$\frac{1}{2}J + 2V + 4\mu$	$\frac{1}{2}J + 2V + 4\mu$

TABLE III: Diagonal matrix blocks of the unrenormalized three-site Hamiltonian $-\beta H(i, j) - \beta H(j, k)$. The Hamiltonian being invariant under spin-reversal, the spin-flipped matrix elements are not shown. The additive constant contribution $2G$, occurring at the diagonal terms, is also not shown. The additional Δ_i terms, which are not part of the original three-site Hamiltonian, are explained in Sec.IIIC.

	ϕ_1	ϕ_2	ϕ_4	ϕ_6	ϕ_7	ϕ_9
ϕ_1	G'					
ϕ_2	$-t' \cos \phi' + \mu' + G'$	$it' \sin \phi'$				0
ϕ_4	$-it' \sin \phi'$	$t' \cos \phi' + \mu' + G'$				
ϕ_6			$-\frac{3}{4}J' + V'_2 + 2\mu' + G'$			
ϕ_7		0		$\frac{1}{4}J' + V'_2 + 2\mu' + G'$		
ϕ_9						$\frac{1}{4}J' + V'_2 + 2\mu' + G'$

TABLE IV: Block-diagonal matrix of the renormalized two-site Hamiltonian $-\beta' H'(i, k)$. The Hamiltonian being invariant under spin-reversal, the spin-flipped matrix elements are not shown.

tonian with interaction constants $\mathbf{K} = \{G, t, J, V, \mu, \phi\}$ onto another Hamiltonian with interactions constants

$$\mathbf{K}' = \mathbf{R}(\mathbf{K}). \quad (13)$$

The Migdal-Kadanoff procedure [18, 19] is used to construct the renormalization-group transformation for $d > 1$. We ignore a subset of the nearest-neighbor interactions in the d -dimensional hypercubic lattice, leaving behind a new d -dimensional hypercubic lattice where each point is connected to its neighbor by two consecutive nearest-neighbor segments of the original lattice. We apply the

decimation described above to the middle site between the two consecutive segments, giving the renormalized nearest-neighbor couplings for the points in the new lattice. We compensate for the interactions that are ignored in the original lattice by multiplying by a factor of b^{d-1} the interactions after the decimation, $b = 2$ being the length rescaling factor. Thus, the renormalization-group transformation of Eq. (13) generalizes, for $d > 1$, to

$$\mathbf{K}' = b^{d-1} \mathbf{R}(\mathbf{K}). \quad (14)$$

B. Renormalization-Group Transformation in the Presence of Magnetic Flux

In order to correctly model the response of the system to an applied magnetic flux, the renormalization-group approximation described in the last two sections needs to be extended. To see this, we first review the formalism for calculating thermodynamic densities from the renormalization-group flows.[20] Conjugate to each interaction K_α of $\mathbf{K} = \{K_\alpha\}$, there is a density M_α (e.g., kinetic energy, electron density),

$$M_\alpha = \frac{1}{Nd} \frac{\partial \ln Z}{\partial K_\alpha}, \quad (15)$$

where $Z(\mathbf{K})$ is the partition function. We can relate the densities at the two consecutive points along a renormalization-group trajectory by

$$M_\alpha = b^{-d} M'_\beta T_{\beta\alpha}, \quad \text{where} \quad T_{\beta\alpha} \equiv \frac{\partial K'_\beta}{\partial K_\alpha}, \quad (16)$$

with summation over repeated indices implied. At a fixed point of the renormalization-group transformation, corresponding to a phase transition or a phase sink, the densities $M_\alpha = M'_\alpha \equiv M_\alpha^*$ are the left eigenvector with eigenvalue b^d of the recursion matrix \mathbf{T} evaluated at the fixed point. The densities at the starting point of the trajectory (the actual physical system) are computed by iterating Eq. (16) until a fixed point is effectively reached. If $\mathbf{T}^{(k)}$ is the recursion matrix of the (k) th renormalization-group iteration, then for large k , we can express the densities of the actual system \mathbf{M} as

$$\mathbf{M} \simeq b^{-kd} \mathbf{M}^* \cdot [\mathbf{T}^{(k)}] \cdot [\mathbf{T}^{(k-1)}] \cdot \dots \cdot [\mathbf{T}^{(1)}]. \quad (17)$$

The renormalization-group transformation incorporated in Eqs. (9)-(14) gives

$$\begin{aligned} \frac{\partial t'}{\partial \phi} = \frac{\partial J'}{\partial \phi} = \frac{\partial V'}{\partial \phi} = \frac{\partial G'}{\partial \phi} = 0, \\ \frac{\partial \phi'}{\partial t} = \frac{\partial \phi'}{\partial J} = \frac{\partial \phi'}{\partial V} = \frac{\partial \phi'}{\partial \mu} = 0, \quad \frac{\partial \phi'}{\partial \phi} = 2, \end{aligned} \quad (18)$$

for all ϕ . The 6×6 recursion matrix \mathbf{T} will then have

the form

$$\mathbf{T} = \left(\begin{array}{cccc|c} b^d & \frac{\partial G'}{\partial t} & \cdots & \frac{\partial G'}{\partial \mu} & 0 \\ 0 & \frac{\partial t'}{\partial t} & \cdots & \frac{\partial t'}{\partial \mu} & \\ \vdots & \vdots & \ddots & \vdots & \\ 0 & \frac{\partial \mu'}{\partial t} & \cdots & \frac{\partial \mu'}{\partial \mu} & \\ \hline & 0 & & & 2 \end{array} \right) \quad (19)$$

at every step in the flow. This leads to

$$M_6^* = 0 \quad \text{and} \quad \frac{\partial}{\partial \phi} \ln Z = M_6 = 0, \quad (20)$$

for all points of the phase diagram. This superfluid weight of zero for all temperatures and electronic densities is clearly due to the oversimplification in our initial approximation.

The source of the problem is the three-site cluster approximation used in deriving the recursion relations. In modifying the original approximation scheme, we seek to incorporate the effect of the non-commutations extending beyond the three-site cluster. Turning to the matrix elements of $-\beta H(i, j) - \beta H(j, k)$ listed in Table III, we note the terms Δ_i , $i = 1, \dots, 4$. Using the original Hamiltonian of Eq. (3) restricted to the three-cluster, the matrix elements involving these terms are all zero. However, non-commutativity extending beyond the three-cluster makes, as we see below, these matrix elements non-zero.

We can estimate the magnitude of the matrix elements Δ_i by considering a five-site cluster, described by Hamiltonian $-\beta H(h, i) - \beta H(i, j) - \beta H(j, k) - \beta H(k, l)$, where (h, i, j, k, l) are consecutive sites. In the spirit of Eq. (8), we generate effective couplings for the three-cluster by tracing over the degrees of freedom at the outside sites in the five-cluster,

$$\begin{aligned} \langle u_i v_j w_k | e^{-\tilde{\beta} \tilde{H}(i, j, k)} | \bar{u}_i \bar{v}_j \bar{w}_k \rangle = \\ \sum_{t_h, x_l} \langle t_h u_i v_j w_k x_l | e^{-\beta H(h, i) - \beta H(i, j) - \beta H(j, k) - \beta H(k, l)} \\ \cdot | t_h \bar{u}_i \bar{v}_j \bar{w}_k x_l \rangle, \quad (21) \end{aligned}$$

where the subscripted variables refer to single-site states. From the above equation, we can extract the matrix elements of an effective three-cluster Hamiltonian $-\tilde{\beta} \tilde{H}(i, j, k)$. Eq. (21) is the contraction of a 243×243 matrix on the right-hand side into a 27×27 matrix on the left. We simplify our task by using the $\{\psi_p\}$ basis on the left, and choosing an appropriate five-site basis to block-diagonalize the 243×243 right-hand matrix.

Since $-\tilde{\beta} \tilde{H}(i, j, k)$ is derived from the decimation of a five-cluster, it will have a more general form than $-\beta H(i, j) - \beta H(j, k)$, and approximately reflect the effect of the three-cluster non-commutations with the external sites. However our approximation scheme must also satisfy an important constraint: the $\phi \rightarrow 0$ limit should yield the same renormalization-group transformation used in earlier studies of the tJ model [10, 11]. To

achieve this, we modify only a subset of the matrix elements of $-\beta H(i, j) - \beta H(j, k)$, namely those which are zero in the original scheme when $\phi \neq 0$, but whose corresponding elements in $-\tilde{\beta} \tilde{H}(i, j, k)$ are non-zero:

$$\begin{aligned} \Delta_1 &= \text{sign}(\phi t) |\langle \psi_3 | \tilde{\beta} \tilde{H}(i, j, k) | \psi_6 \rangle|, \\ \Delta_2 &= \text{sign}(\phi t) |\langle \psi_{12} | \tilde{\beta} \tilde{H}(i, j, k) | \psi_{17} \rangle|, \\ \Delta_3 &= \text{sign}(\phi t) |\langle \psi_8 | \tilde{\beta} \tilde{H}(i, j, k) | \psi_9 \rangle|, \\ \Delta_4 &= \text{sign}(\phi t) |\langle \psi_{13} | \tilde{\beta} \tilde{H}(i, j, k) | \psi_{18} \rangle|. \end{aligned} \quad (22)$$

The $\text{sign}(\phi t)$ prefactors guarantee that couplings between the same types of three-cluster states have the same sign. For example, $|\psi_2\rangle$ and $|\psi_3\rangle$ share the same n , p , s , and m_s quantum numbers, as can be seen from Table II. A nonzero ϕ couples $|\psi_2\rangle$ to $|\psi_6\rangle$, a state with the same n , s , and m_s , but opposite parity. From the second block in Table III, the associated matrix element is $\langle \psi_2 | \cdots | \psi_6 \rangle = i\sqrt{2}t \sin(\phi)$. The Δ_1 elements in that block have an analogous role, coupling $|\psi_3\rangle$ to $|\psi_6\rangle$. The prefactor in the Δ_1 expression of Eq. (22) sets the sign of the element $\langle \psi_3 | \cdots | \psi_6 \rangle = i\Delta_1$ to equal that of $\langle \psi_2 | \cdots | \psi_6 \rangle$. Since our calculations are all done for small ϕ , $\text{sign}(\sin \phi) = \text{sign}(\phi)$. Similar reasoning applies to the prefactors of the other Δ_i elements.

Through Eq. (21), the Δ_i are functions of the interactions strengths in the unrenormalized Hamiltonian, $\Delta_i = \Delta_i(t, J, V, \mu, \phi)$. They scale like ϕ for small ϕ , and duly vanish in the limit $\phi \rightarrow 0$. As will be explained in Sec. III E, finding the superfluid weight involves calculating a thermodynamic density in the $\phi \rightarrow 0$ limit, so we shall be working in the regime where the Δ_i are vanishingly small. The result of the extended calculation, taking into account the quantum mechanical backflow into the three-cluster, is that Eqs. (18) no longer hold, $\partial \ln Z / \partial \phi \neq 0$ in general, and we obtain interesting non-trivial results for n_s / m^* .

C. Calculation of the Superfluid Weight

The superfluid weight of Eq. (4) is expressed as a derivative of the total free energy $F = F(n, T, \phi)$, where $n = \langle n_i \rangle$ is the electron density. In terms of the conjugate current

$$j(n, T, \phi) = \frac{1}{Nd} \left. \frac{\partial F}{\partial \phi} \right|_{n, T}, \quad (23)$$

Eq. (4) becomes

$$\frac{n_s}{m^*}(n, T) = \lim_{\phi \rightarrow 0} \left. \frac{\partial j}{\partial \phi} \right|_{n, T}. \quad (24)$$

In terms of the grand potential $\Omega(\mu, T, \phi) = -(1/\beta) \ln Z$,

$$j(\mu, T, \phi) = \frac{1}{Nd} \left. \frac{\partial \Omega}{\partial \phi} \right|_{\mu, T}, \quad (25)$$

and

$$n(\mu, T, \phi) = -\frac{\beta}{2Nd} \frac{\partial \Omega}{\partial \mu} \Big|_{T, \phi}. \quad (26)$$

Relating the partial derivatives of j with respect to ϕ through

$$\frac{\partial j}{\partial \phi} \Big|_{\mu, T} = \frac{\partial j}{\partial n} \Big|_{\phi, T} \frac{\partial n}{\partial \phi} \Big|_{\mu, T} + \frac{\partial j}{\partial \phi} \Big|_{n, T}, \quad (27)$$

and using the Maxwell relation $\frac{\partial n}{\partial \phi} \Big|_{\mu, T} = -\frac{\beta}{2} \frac{\partial j}{\partial \mu} \Big|_{\phi, T}$,

$$\frac{\partial j}{\partial \phi} \Big|_{\mu, T} = -\frac{\beta}{2} \frac{\partial j}{\partial n} \Big|_{\phi, T} \frac{\partial j}{\partial \mu} \Big|_{\phi, T} + \frac{\partial j}{\partial \phi} \Big|_{n, T}. \quad (28)$$

The current j is zero when $\phi = 0$, so that the first term on the right-hand side above is also zero in the limit $\phi \rightarrow 0$, and we find that $\lim_{\phi \rightarrow 0} \frac{\partial j}{\partial \phi} \Big|_{\mu, T} = \lim_{\phi \rightarrow 0} \frac{\partial j}{\partial \phi} \Big|_{n, T}$. Thus Eq. (24) can be equivalently written as

$$\begin{aligned} \frac{n_s}{m^*}(\mu, T) &= \lim_{\phi \rightarrow 0} \frac{\partial j}{\partial \phi} \Big|_{\mu, T} = \frac{1}{Nd} \lim_{\phi \rightarrow 0} \frac{\partial^2 \Omega}{\partial \phi^2} \Big|_{\mu, T} \\ &= -\frac{1}{\beta Nd} \lim_{\phi \rightarrow 0} \frac{\partial^2 \ln Z}{\partial \phi^2} \Big|_{\mu, T}. \end{aligned} \quad (29)$$

This is the form we shall use when calculating the superfluid weights.

IV. RESULTS

A. Global Phase Diagram for $d = 3$

Each sink, or completely stable fixed point of the renormalization-group flows, corresponds to a thermodynamic phase, and we find the global phase diagram by determining the basin of attraction for every sink [21]. Flows that start at the boundaries between phases have their own fixed points, distinguished from phase sinks by having at least one unstable direction. Analysis of these fixed points determines whether the phase transition is first- or second-order. As explained in Sec. III C, the thermodynamic densities, which are the expectation values of operators occurring in the Hamiltonian, can also be calculated from the renormalization-group flows. In particular, we determine the single-site electron density $\langle n_i \rangle$. For the coupling $J/t = 0.444$ and $\phi = 0$, the phase diagram in terms of $\langle n_i \rangle$ and temperature $1/t$ is shown in Fig. 1 [10, 11].

The nature of the various phases is epitomized by the thermodynamic densities \mathbf{M}^* calculated at each phase sink (Table V), which underpin the calculation of densities throughout their respective phases (Eq. (17)). We summarize the phase properties below (for a more detailed discussion, see [10, 11]):

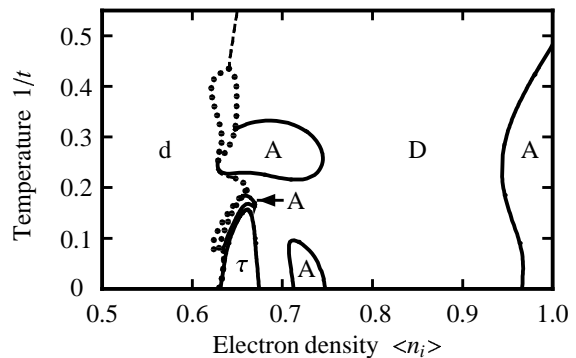


FIG. 1: Phase diagram for the $d = 3$ tJ model with $J/t = 0.444$, $\phi = 0$, in temperature versus electron density.[10] The antiferromagnetic (A), dense disordered (D), dilute disordered (d), and τ phases are seen. The second-order phase boundaries are drawn with full curves. The coexistence boundaries of first-order transitions are drawn with dotted curves, with the unmarked areas inside corresponding to coexistence regions of the two phases at either side. The dashed lines are not phase transitions, but disorder lines between the dilute disordered and dense disordered phases.

Phase sink	Expectation values			
	$\sum_{\sigma} \langle c_{i\sigma}^{\dagger} c_{j\sigma} + c_{j\sigma}^{\dagger} c_{i\sigma} \rangle$	$\langle n_i \rangle$	$\langle \mathbf{S}_i \cdot \mathbf{S}_j \rangle$	$\langle n_i n_j \rangle$
d	0	0	0	0
D	0	1	0	1
A	0	1	$\frac{1}{4}$	1
τ	$-\frac{2}{3}$	$\frac{2}{3}$	$-\frac{1}{4}$	$\frac{1}{3}$

TABLE V: Expectation values at the phase-sink fixed points.

Dilute disordered phase (d): The electron density $\langle n_i \rangle = 0$ at the sink and, as a result, the $\langle n_i \rangle$ calculated inside this phase are low.

Dense disordered phase (D): The electron density $\langle n_i \rangle = 1$ at the sink and, as a result, the $\langle n_i \rangle$ calculated inside this phase are close to 1.

Antiferromagnetic phase (A): The electron density $\langle n_i \rangle = 1$ at the sink, so that this phase is also densely filled. The nearest-neighbor spin-spin correlation $\langle \mathbf{S}_i \cdot \mathbf{S}_j \rangle = 1/4$ at the sink. Two spins that are nearest neighbors at the sink are distant members of the same sublattice in the original cubic lattice. The non-zero value of the correlation function at the sink leads to $\langle \mathbf{S}_i \cdot \mathbf{S}_j \rangle < 0$ for nearest-neighbor sites of the original, unrenormalized system.

τ phase: This is a novel phase, characterized by partial-filling at the phase sink, $\langle n_i \rangle = 2/3$. It is the only phase where the electron hopping strength t does not renormalize to zero after repeated rescalings; instead, $t \rightarrow \infty$ at the sink. As a result, the expectation value of the electron hopping operator at the sink is non-zero, $\sum_{\sigma} \langle c_{i\sigma}^{\dagger} c_{j\sigma} + c_{j\sigma}^{\dagger} c_{i\sigma} \rangle = -2/3$. This property makes it a possible tJ model analogue to the superconducting phase in high- T_c materials. The superfluid weight and thermo-

dynamic results discussed below certainly support this idea.

In the limit $\langle n_i \rangle = 1$, the system exhibits antiferromagnetic order at low temperatures, as expected from the spin-spin coupling in the Hamiltonian. Upon hole doping, there is a competition between the A and D phases, which respectively minimize antiferromagnetic potential energy and hole kinetic energy. Note the extent of the A phase near $\langle n_i \rangle = 1$, which persists only up to a small amount of hole doping $\delta = 1 - \langle n_i \rangle \lesssim 0.05$. This feature is directly reminiscent of the antiferromagnetic phase in certain high- T_c materials, for example $\text{La}_{2-x}\text{Sr}_x\text{CuO}_4$ [22]. At intermediate dopings $\delta \approx 0.32 - 0.37$, we have a low-temperature τ phase, surrounded by islands of antiferromagnetism. (When the hopping strength t increases under rescaling, this also lowers the free energy of antiferromagnetically long-range ordered states, which leads to these islands of A in the vicinity of the τ phase.[10]) At hole dopings $\delta \gtrsim 0.37$, there is a transition to a dilute disordered phase, with a narrow region of first-order coexistence at lower temperatures.

B. Superfluid Weight and Kinetic Energy

Using the method of calculating thermodynamic densities described in Sec.IIIE, we determine $(1/Nd)\partial \ln Z/\partial \phi$ at small ϕ . Taking the numerical derivative of this quantity at $\phi = 0$, we find n_s/m^* through Eq. (29). The superfluid weight is plotted as a function of electron density in Fig. 2, along four different constant temperature cross-sections of the phase diagram. For comparison, we also show in the same figure the calculated average kinetic energy per bond $\langle K \rangle$, where $K = -\sum_{\sigma} (c_{i\sigma}^{\dagger} c_{j\sigma} + c_{j\sigma}^{\dagger} c_{i\sigma})$. $\langle K \rangle$ and the total weight of $\sigma_1(\omega, T)$, the real part of the optical conductivity, are related by the sum rule [23],

$$\int_0^{\infty} d\omega \sigma_1(\omega, T) = \frac{\pi e^2}{2} \langle K \rangle. \quad (30)$$

In comparing the properties of the tJ model to those of high- T_c materials, we keep in mind that the tJ Hamiltonian describes a one-band model, so cannot account for interband transitions. For real materials, the full conductivity sum rule has the form

$$\int_0^{\infty} d\omega \sigma_1(\omega, T) = \frac{\pi e^2 n}{2m}, \quad (31)$$

where n is the total density of electrons and m is the free electron mass. The right-hand side of Eq. (31) is independent of electron-electron interactions, in contrast to the right-hand side of Eq. (30), where $\langle K \rangle$ will vary with the interaction strengths in the Hamiltonian. The optical conductivity of actual materials incorporates both transitions within the conduction band and those to higher bands, while the tJ model contains only the conduction band. We can look at Eq. (30) as a partial sum

rule [23, 24], which reflects the spectral weight of the free carriers in the conduction band.

The experimental quantity we are interested in modeling is the effective density of free carriers, which in actual materials is calculated from the low-frequency spectral weight [25],

$$n_{\text{free}}(T) = \frac{2m}{\pi e^2} \int_0^{\omega_0} d\omega \sigma_1(\omega, T). \quad (32)$$

For high T_c materials, the cutoff frequency is typically chosen around $\hbar\omega_0 \approx 1$ eV so as to include only intra-band transitions. For comparison with the tJ model, we identify the right-hand side of Eq. (30) with

$$\frac{\pi e^2}{2} \langle K \rangle = \frac{\pi e^2 n_{\text{free}}(T)}{2m}. \quad (33)$$

The superfluid weight satisfies the inequality [26]

$$\frac{n_s}{m^*} \leq \langle K \rangle = \frac{n_{\text{free}}}{m}, \quad (34)$$

which is obeyed in our results in Fig.2.

The superfluid weight graphs at the sampled temperatures show a clear bipartite structure, with a peak at low $\langle n_i \rangle$, and another peak at high $\langle n_i \rangle$ (which develops into two closely spaced peaks at lower temperatures). In between these is a region of low superfluid weight, with a minimum near $\langle n_i \rangle \simeq 0.385$, approximately independent of temperature. Looking at the nearest-neighbor density-density correlation $\langle n_i n_j \rangle$ as shown in Fig. 3, we see that $\langle n_i \rangle \simeq 0.385$ is also the electron density separating two different regimes of the system: an extremely dilute regime, where $\langle n_i n_j \rangle \simeq 0$, and a partially-to-densely filled regime, where $\langle n_i n_j \rangle > 0$. It is therefore useful to discuss the superfluid weight and kinetic energy results in terms of these two regimes.

1. Extremely dilute regime, $\langle n_i \rangle \lesssim 0.385$

The system in this regime is a dilute gas of electrons. For low $\langle n_i \rangle$, the kinetic energy per bond $\langle K \rangle \simeq 2\langle n_i \rangle$, which follows if the density of free carriers is just the density of electrons, $n_{\text{free}} = \langle n_i \rangle$, and the mass of the carriers $m = 1/2$. The interaction terms in the tJ Hamiltonian create an attractive potential of strength $-\tilde{J}$ between electrons in singlet-states on neighboring sites. For a coupling $J/t = 0.444$, this attraction is too weak to form two-body bound states, but since we are in three dimensions, even a weak attractive potential is sufficient for the formation of an electron superfluid at low temperatures [27, 28]. In fact, we see a peak in n_s/m^* develop around $\langle n_i \rangle \approx 0.3-0.35$, and this peak grows as the temperature is lowered from $1/t = 0.315$ to 0.1. For low $\langle n_i \rangle$, the superfluid weight increases with electron density and $\langle K \rangle$. The location of the peak in n_s/m^* is just before $\langle K \rangle$ comes to its maximum and levels off. As the

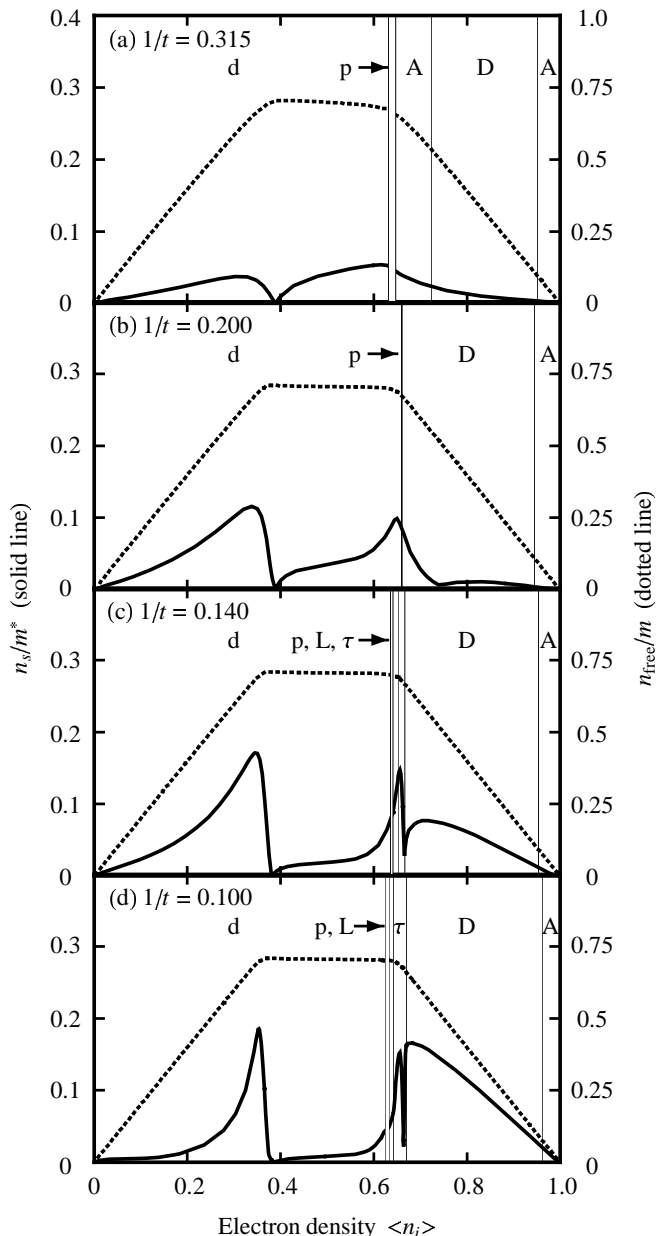


FIG. 2: The superfluid weight n_s/m^* (solid line) and free carrier density n_{free}/m (dotted line) as a function of electron density at four different values of temperature $1/t$. The corresponding phases are indicated above the plots, and the location of phase boundaries marked by thin vertical lines. The symbol p refers to a region of forbidden densities due to the discontinuity at a first-order transition. The symbol L refers to a “lamellar” region where narrow slivers of the A and D phases alternate.

density of free carriers saturates near $\langle n_i \rangle \simeq 0.385$, there is a sharp drop in n_s/m^* , and $\langle n_i n_j \rangle$ begins to increase from zero. At this density the physical characteristics of the system abruptly change, without however inducing a phase transition.

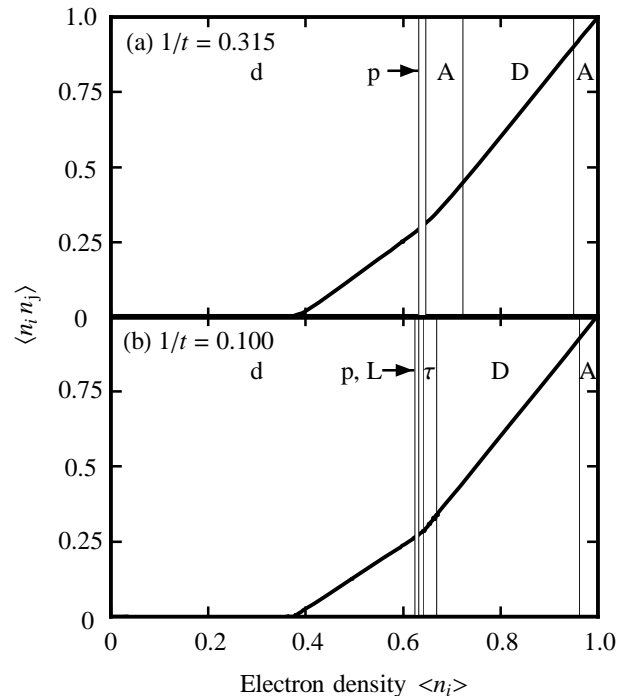


FIG. 3: The nearest-neighbor density-density correlation $\langle n_i n_j \rangle$ as a function of electron density at two different values of temperature $1/t$. The corresponding phases are indicated above the plots, and the location of phase boundaries marked by thin vertical lines. The symbol p refers to a region of forbidden densities due to the discontinuity at a first-order transition. The symbol L refers to a “lamellar” region where narrow slivers of the A and D phases alternate.

2. Partially-to-densely filled regime, $\langle n_i \rangle \gtrsim 0.385$

For intermediate densities $\langle n_i \rangle \approx 0.385$ – 0.63 , the kinetic energy $\langle K \rangle$ remains approximately constant. Near $\langle n_i \rangle \simeq 0.63$, there is a phase transition to a densely filled phase (either D or A). We go from a physical picture where the carriers are electrons in a mostly empty background to one where the carriers are holes moving in a mostly filled background. These holes condense into a superfluid at lower temperatures, and the peak in n_s/m^* occurs in the vicinity of the dilute-dense narrow first-order phase transition. For $1/t \lesssim 0.16$, the maximum superfluid weight is reached inside the τ phase. In the densely filled regime, $\langle n_i \rangle \gtrsim 0.63$, the kinetic energy goes linearly as $\langle K \rangle \simeq 2(1 - \langle n_i \rangle) = 2\delta$, as expected if the free carriers are holes.

For hole-doped high- T_c materials, the density of free carriers increases with δ until the doping level optimal for superconductivity is reached, and remains approximately constant in the overdoped regime.[6] The superfluid weight, in contrast, peaks near optimal doping and sharply decreases with overdoping. These trends are reproduced in our numerical results, identifying, from our calculated n_s/m^* maxima, the optimal doping for the tJ model as $\delta \approx 0.32$ – 0.37 , the range of densities where the τ

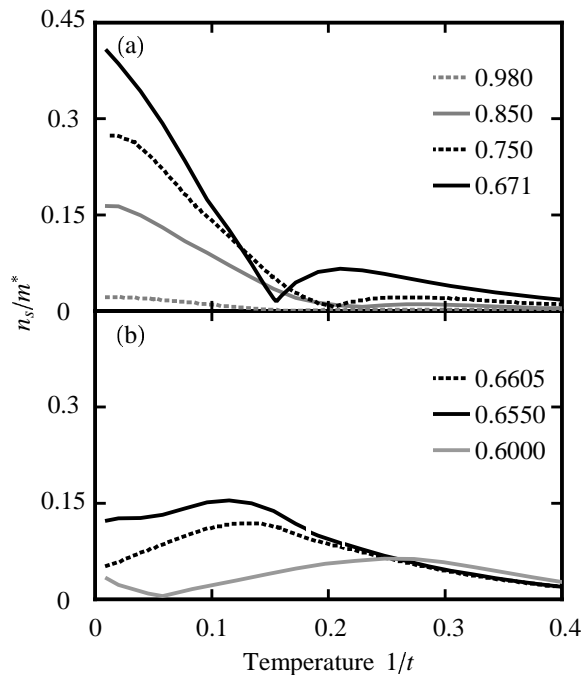


FIG. 4: The superfluid weight n_s/m^* as a function of temperature $1/t$ for various electron densities $\langle n_i \rangle$ indicated in the legends. Fig. 4(a) shows results in the range of small to optimal hole doping, while Fig. 4(b) shows results for hole overdoped systems.

phase occurs. Note that optimal doping for high- T_c materials is lower than this, typically around $\delta = 0.15$, and the closely spaced double-peak structure of n_s/m^* at low temperatures near optimal doping is not observed. On the other hand, our approximation for the $d = 3$ tJ model is closer to experiment in this respect than earlier numerical studies of the tJ model, which focused mostly on finite-cluster techniques applied to the $d = 2$ system [29]. In these earlier studies optimal doping is identified near $\langle n_i \rangle = 0.5$ on the basis of d-wave pairing correlations and the peak in the superfluid weight [9]. Also in these earlier studies, the kinetic energy has a maximum at $\langle n_i \rangle = 0.5$, but, unlike experiments, does not saturate with overdoping [30].

To complete the description of the superfluid weight in this regime, in Fig. 4 we show n_s/m^* as a function of temperature $1/t$ at various electron densities $\langle n_i \rangle$. For systems with small to optimal hole dopings, shown in Fig. 4(a), there is a clear onset temperature near $1/t \simeq 0.2$ below which the superfluid weight rises rapidly, until it levels off near zero temperature. This behavior is in good comparison with experimental results with $\text{YBa}_2\text{Cu}_3\text{O}_{6+x}$ [31]. As we move past optimal doping to the overdoped systems of Fig. 4(b), we see a marked change in behavior, with the low temperature n_s/m^* suppressed.

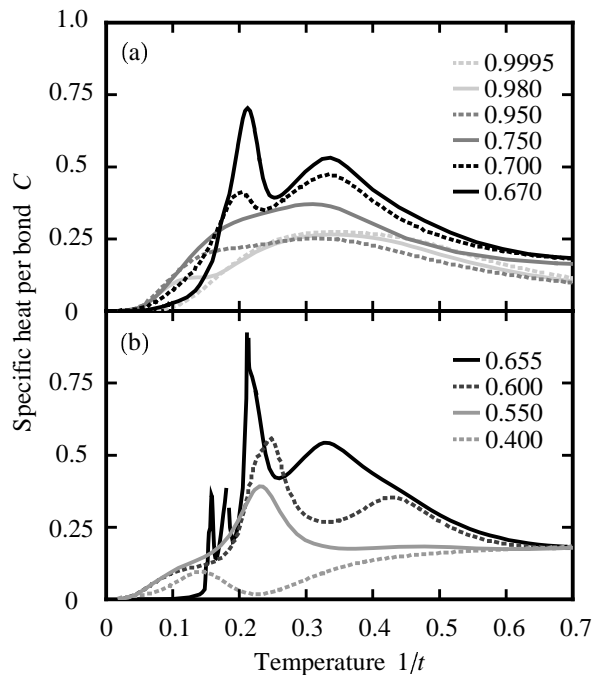


FIG. 5: The specific heat per bond C , in units of k_B , as a function of temperature $1/t$ for various electron densities $\langle n_i \rangle$ (indicated in the legends). Fig. 5(a) shows results in the range of small to optimal hole doping, while Fig. 5(b) shows results for hole overdoped systems. The small discontinuities in the plot for $\langle n_i \rangle = 0.655$ reflect temperature ranges where that particular density does not appear because of the narrow first-order phase transition.

C. Specific Heat

Since the superfluid weight peaks inside the τ phase at low temperatures, it is interesting to check whether the τ region has any other general characteristics of a superconducting phase. We have added a magnetic field spin coupling term to the tJ Hamiltonian and have shown that the τ phase continues to exist when $H \neq 0$, up to a critical field $H_c(T)$, which decreases with increasing temperature and goes to zero at the temperature of the τ phase boundary. In our present study, we look at the spectrum of excitations of the system through the specific heat per bond

$$C(n, T) = \left. \frac{\partial \langle H(i, j) \rangle}{\partial T} \right|_n, \quad (35)$$

calculated for $\phi = 0$. If the τ phase corresponds to the superconducting phase in real materials, we should see evidence of a gap in the excitation spectrum.

The results for C as a function of temperature $1/t$ are plotted in Fig. 5 for a series of different electronic densities $\langle n_i \rangle$. Starting at $\langle n_i \rangle = 0.9995$, the smallest hole doping shown in Fig. 5(a), we observe a broad peak around $1/t \simeq 0.33$, corresponding to $k_B T \simeq 0.75\tilde{J}$. We can identify this peak with the thermal excitation of the

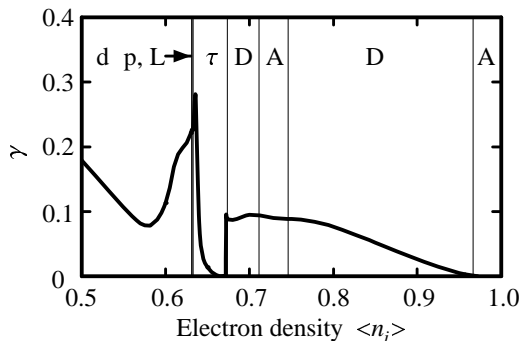


FIG. 6: The specific heat coefficient $\gamma = C/T$, in units of k_B^2 , as a function of electron density $\langle n_i \rangle$ at temperature $1/t = 0.015$. The corresponding phases are indicated above the plot, and the location of phase boundaries marked by thin vertical lines. The symbol p refers to a region of forbidden densities due to the narrow discontinuity at a first-order transition. The symbol L refers to a “lamellar” region where narrow slivers of the A and D phases alternate.

spin degrees of freedom. As we dope the system with holes, the weight under the curve at lower temperatures increases due to excitation of charge degrees of freedom. As we approach optimal doping, a second peak develops around $1/t \simeq 0.2$. Note that this approximately coincides with the onset temperature below which we see a dramatic increase in n_s/m^* in Fig. 4. The spin-excitation peak is also enhanced for $\langle n_i \rangle \approx 0.65\text{--}0.75$, which is related to the appearance of an antiferromagnetic island around $1/t \simeq 0.3$ in that density range.

The peak at $1/t \simeq 0.2$ grows rapidly near optimal doping, reminiscent of the specific heat anomaly of high- T_c materials [32, 33]. For $\langle n_i \rangle = 0.655$ we see the appearance of two subsidiary peaks below the main one at $1/t \simeq 0.2$. These smaller peaks may be related to the complicated lamellar structure of A and D regions above the τ phase boundary. For temperatures $1/t \lesssim 0.16$, inside the τ phase, the specific heat is strongly suppressed, reflecting the opening up of a gap in the excitation spectrum. We can see this gap more directly by looking at the low-temperature limit of the specific heat. Quasiparticle excitations contribute a linear term to the specific

heat $C \simeq \gamma T$ for small T . In Fig. 6, we plot $\gamma = C/T$ as a function of electron density at a low temperature, $1/t = 0.015$. The specific heat coefficient $\gamma \simeq 0$ in the A phase near half-filling, but then grows with increasing hole doping. At the onset of the τ phase a gap opens in the quasiparticle spectrum, γ falls sharply, and stays small until it rises again near the phase boundary. Qualitatively, this doping-dependence of the low-temperature specific heat coefficient agrees well with the experimental results for high- T_c superconducting materials [32].

V. CONCLUSIONS

We have developed a position-space renormalization-group approximation to study the superfluid weight of the three-dimensional tJ model. Our results indicate that optimal hole doping for this system occurs in the density range of the τ phase, $\langle n_i \rangle \approx 0.63\text{--}0.68$, where n_s/m^* reaches a local maximum. While the superfluid weight drops off sharply in the overdoped region, the density of free carriers, proportional to the kinetic energy, remains approximately constant, as seen experimentally in high- T_c materials. From calculations of the specific heat coefficient γ , we see clear evidence of a gap in the excitation spectrum for the τ phase. Earlier renormalization group studies [10, 11] had suspected that the τ phase corresponds to the superconducting phase of high- T_c materials, and this idea was reinforced when an analogous phase was discovered in the Hubbard model [12, 13]. Our present results justify this suspicion.

Acknowledgments

This research was supported by the U.S. Department of Energy under Grant No. DE-FG02-92ER-45473, by the Scientific and Technical Research Council of Turkey (TÜBİTAK) and by the Academy of Sciences of Turkey. MH gratefully acknowledges the hospitality of the Feza Gürsey Research Institute and of the Physics Department of Istanbul Technical University.

-
- [1] Y.J. Uemura, G.M. Luke, B.J. Sternlieb, J.H. Brewer, J.F. Carolan, W.N. Hardy, R. Kadono, J.R. Kempton, R.F. Kiefl, S.R. Kreitzman, P. Mulhern, T.M. Riseman, D.L. Williams, B.X. Yang, S. Uchida, H. Takagi, J. Gopalakrishnan, A.W. Sleight, M.A. Subramanian, C.L. Chien, M.Z. Cieplak, G. Xiao, V.Y. Lee, B.W. Statt, C.E. Stronach, W. J. Kossler, and X.H. Yu, Phys. Rev. Lett. **62**, 2317 (1989).
 - [2] C. Bernhard, C. Niedermayer, U. Binniger, A. Hofer, C. Wenger, J.L. Tallon, G.V.M. Williams, E.J. Ansaldo, J.I. Budnick, C.E. Stronach, D.R. Noakes, and M.A. Blankson-Mills, Phys. Rev. B **52**, 10488 (1995).
 - [3] C. Niedermayer, C. Bernhard, U. Binniger, H. Glückler, J.L. Tallon, E.J. Ansaldo, and J.I. Budnick, Phys. Rev. Lett. **71**, 1764 (1993).
 - [4] J.P. Locquet, Y. Jaccard, A. Cretton, E.J. Williams, F. Arrouy, E. Mächler, T. Schneider, Ø. Fischer, and P. Martinoli, Phys. Rev. B **54**, 7481 (1996).
 - [5] C. Bernhard, J.L. Tallon, T. Blasius, A. Gornik, and C. Niedermayer, Phys. Rev. Lett. **86**, 1614 (2001).
 - [6] A.V. Puchkov, P. Fournier, T. Timusk, and N.N. Kolesnikov, Phys. Rev. Lett. **77**, 1853 (1996).
 - [7] S.-S. Lee and S.-H.S. Salk, Phys. Rev. B **64**, 052501 (2001).

- [8] S.-S. Lee and S.-H.S. Salk, cond-mat/0212582.
- [9] E. Dagotto and J. Riera, Phys. Rev. Lett. **70**, 682 (1993).
- [10] A. Falicov and A.N. Berker, Phys. Rev. B **51**, 12458 (1995).
- [11] A. Falicov and A.N. Berker, Turk. J. Phys. **19**, 127 (1995).
- [12] G. Migliorini and A.N. Berker, Eur. Phys. J. B **17**, 3 (2000).
- [13] M. Hinczewski and A.N. Berker, cond-mat/0503226.
- [14] M.E. Fisher, M.N. Barber, and D. Jasnow, Phys. Rev. A **8**, 1111 (1973).
- [15] D.J. Scalapino, S.R. White, and S. Zhang, Phys. Rev. B **47**, 7995 (1993).
- [16] M. Suzuki and H. Takano, Phys. Lett. A **69**, 426 (1979).
- [17] H. Takano and M. Suzuki, J. Stat. Phys. **26**, 635 (1981).
- [18] A.A. Migdal, Zh. Eksp. Teor. Fiz. **69**, 1457 (1975) [Sov. Phys. JETP **42**, 743 (1976)].
- [19] L.P. Kadanoff, Ann. Phys. (N.Y.) **100**, 359 (1976).
- [20] A.N. Berker, S. Ostlund, and F.A. Putnam, Phys. Rev. B **17**, 3650 (1978).
- [21] A.N. Berker and M. Wortis, Phys. Rev. B **14**, 4946 (1976).
- [22] M. Imada, A. Fujimori, and Y. Tokura, Rev. Mod. Phys. **70**, 1039 (1998).
- [23] L. Tan and J. Callaway, Phys. Rev. B **46**, 5499 (1992).
- [24] D. Baeriswyl, C. Gros, and T.M. Rice, Phys. Rev. B **35**, 8391 (1987).
- [25] J. Orenstein, G.A. Thomas, A.J. Millis, S.L. Cooper, D.H. Rapkine, T. Timusk, L.F. Schneemeyer, and J.V. Waszczak, Phys. Rev. B **42**, 6342 (1990).
- [26] A. Paramekanti, N. Trivedi, and M. Randeria, Phys. Rev. B **57**, 11639 (1998).
- [27] V.J. Emery, S.A. Kivelson, and H.Q. Lin, Phys. Rev. Lett. **64**, 475 (1990).
- [28] M. Randeria, J.-M. Duan, and L.-Y. Shieh, Phys. Rev. Lett. **62**, 981 (1989).
- [29] E. Dagotto, Rev. Mod. Phys. **66**, 763 (1994).
- [30] E. Dagotto, A. Moreo, F. Ortolani, D. Poilblanc, and J. Riera, Phys. Rev. B **45**, 10741 (1992).
- [31] Y. Zuev, M.S. Kim, and T.R. Lemberger, cond-mat/0410135.
- [32] J.W. Loram, K.A. Mirza, J.R. Cooper, and W.Y. Liang, Phys. Rev. Lett. **71**, 1740 (1993).
- [33] J.W. Loram, K.A. Mirza, J.M. Wade, J.R. Cooper, and W.Y. Liang, Physica C **235-240**, 134 (1994).